Original article

Institution of MECHANICAL ENGINEERS
Journal of AUTOMOBILE ENGINEERING

Proc IMechE Part D:
J Automobile Engineering
1–12

DOI: 10.1177/0954407019862913
journals.sagepub.com/home/pid
SAGE

An improved active drag reduction system for formula race cars

Mauro Dimastrogiovanni[1], Giulio Reina[1] and Andrea Burzoni[2]

Abstract

Drag reduction systems are largely employed in racing car competitions to help drivers in overtaking manoeuvres, ensuring a good show to the public. This paper presents a full-design approach to drag reduction systems that includes the computational fluid dynamics estimation of the forces acting on the rear wing, the dynamic analysis of the drag reduction system mechanism and the whole vehicle behaviour through the simulation of an overtaking manoeuvre. For the purposes of this work, a novel drag reduction system mechanism is proposed that features lower aerodynamic disturbance and comparable manufacturing costs than those of drag reduction systems of the main Formula categories.

Keywords

Formula race cars, drag reduction systems, mechanism design, vehicle dynamics, overtaking manoeuvre, aerodynamic efficiency

Date received: 27 December 2018; accepted: 20 June 2019

Introduction

Performance of modern racing Formula cars is strongly affected by aerodynamics, due to their high operating speed. A disturbed front flow due to the wake produced by the rear wing of the preceding vehicle becomes a disadvantage for a car approaching to overtake, resulting in less downforce generated by its front wing. In turn, it translates in less acceleration, deceleration and higher understeer in curve.[1] Especially for Formula One,[2] overtaking has become year by year more difficult and sometimes impossible to be performed.[3]

Different solutions have been introduced in the last few years in order to make overtaking manoeuvres easier.[4] A first idea to increase overtaking by reducing the car wake was represented by the Centre Downwash Generating Wing, developed by FIA (Fédération Internationale de l'Automobile) in 2005 and prototyped by Ferrari. During wind tunnel tests in 2006, this idea did not give the expected results and was rejected.[5] In 2007, the Overtaking Working Group (OWG), a subgroup of engineers from the three top Formula 1 teams of the year, Ferrari, Renault and McLaren, was created with the aim of developing new solutions to address the overtaking problem. Thanks to the OWG work, in the 2009 season, the rear wings were 75% narrower and 150 mm higher; the diffusers were mounted further back; the front wings were lower, wider and with a central sector, the most wake-sensitive, designed with a neutral profile that could not generate downforce. The new front wings included also adjustable flaps, allowing the driver to correct the vehicle balance, changing flap incidence up to $\pm 3°$ only twice a lap. Although all the above changes contributed to lower the sensitivity to turbulence, they resulted as well as in a decrease in the overall car aerodynamic performance in a free-stream (no-wake) condition. For this reason, slick tyres were allowed for the first time since 1997, to compensate the less downforce with a large mechanical grip. In 2009, teams were also able to use Kinetic Energy Recovery Systems (KERS) to recover part of the decelerating energy and use it during overtaking. In these systems, a motor/generator is coupled with the gearbox to absorb energy during braking, storing it in a battery pack and releasing it when claimed by the driver.[6] Two seasons later, in 2011, after the temporary abolition of KERS during 2010, front flap regulation was replaced by the drag reduction system (DRS), even now used, in which the adjustable flap is on the rear

[1]Department of Engineering for Innovation, University of Salento, Lecce, Italy
[2]Dallara, Parma, Italy

Corresponding author:
Giulio Reina, Department of Engineering for Innovation, University of Salento, Via per Arnesano, 73100 Lecce, Italy.
Email: giulio.reina@unisalento.it

wing. The system reduces rear flap incidence, causing a drag drop and a larger acceleration of the car. It is more effective than the front adjustable flap and so its usage is strictly limited. The system can be activated in one or two of the circuit so-called DRS zones, typically included in the two longer circuit straight lines, and only if the preceding car has less than 1 s of advantage. This system allows FIA to adjust, year by year, both DRS zone length and location to reach overtaking targets. DRS is automatically deactivated at either the end of DRS zone or when the driver brakes.[7]

Over the last few years, the potential of using active aerodynamic devices has been investigated in different areas of the automotive field including ride comfort, handling, braking and for pitch control. Improvements in ride comfort have been studied in Savkoor and Hapel[8] that proposed the use of spoilers as active elements of the suspension system to reduce the vibration oscillations of the vehicle chassis. Vehicle handling can also be controlled by introducing corrective yaw moment generated by active aerodynamic devices.[9,10] Another possible application is braking by using the drag force of aerodynamic profiles in order to implement what are referred to as 'air brakes'.[9] Finally, pitch and heave motions of the truck cabin can be appropriately controlled via active airfoils as discussed in Savkoor et al.[11] Although vehicle speeds are much lower, Formula SAE cars can as well take advantage of DRS for engine cooling purposes as described in Schinestzki et al.[12] The aerodynamic stress field that generates across a vertically mounted airfoil can be used to propel lightweight vehicles as explained in Reina and Foglia.[13]

This paper proposes an evolution of DRS for Formula cars that aims to improve aerodynamic efficiency while ensuring cost-effectiveness and ease of maintenance. The performance of a race car endowed with the proposed system are evaluated following a full-design approach where the computational fluid dynamics (CFD) and dynamic behaviour of the whole car are integrated.

Throughout the paper, the x-, y- and z-axis of the vehicle refer, respectively, to the forwards, leftwards and upwards direction.[14]

In the section 'Existing solutions and proposed DRS', existing solutions are compared with the proposed active aerodynamic device that is described in detail. Section 'CFD model validation' presents the validation of the CFD model employed for the evaluation of the aerodynamic stress field acting on the system. The 'Rear-wing CFD model' section describes first the simplified rear wing chosen, made up of constant section of NACA profiles, selected to be near to custom profiles designed by Formula car manufacturers. Then, it illustrates the CFD model of the rear wing used to compute the aerodynamic forces acting on it. The section 'Performance evaluation of the proposed system' presents the results of the flap opening dynamic simulation. In the 'Overtaking manoeuvre' section, the overtaking simulation is performed, verifying the vehicle ability to complete the manoeuvre with DRS assistance on a reference circuit. Finally, in the 'Conclusions and future works' section, relevant conclusions are discussed.

Existing solutions and proposed DRS

The starting point for the choice of a novel DRS is the analysis of past and modern solutions, in order to find a design concept being usable on modern racing cars, which can be a positive evolution or improvement with respect to previous concepts. DRSs are typically provided with hydraulic actuators. This kind of actuator is lighter, cheaper and more reliable than an electric one. A hydraulic actuator could also keep a position without any energy use. It generates less fluid losses and higher piston forces than a pneumatic actuator of the same size. Moreover, a hydraulic system is usually employed on racing cars for gear shifting. For these reasons, in the following research, we will always refer to hydraulic actuators.

The first DRSs in Formula 1 presented a push-up system, in which the actuator was inside a vertical pillar below the mainplane (Figure 1(a)). This system is simple and economic because it requires only a link between actuator and flap, with at most two bearings placed at the link extremities. However, it creates aerodynamic disturbance on the underside of the wing

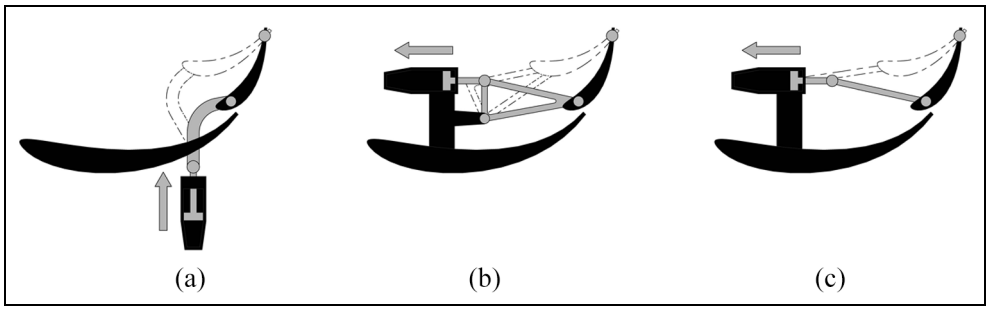

Figure 1. Existing DRS solutions: (a) push-up type, (b) pod-rocker type and (c) pod-pull type (adapted from Scarborough[15]). Closed configuration is shown in filled greyscale view, whereas open configuration is contoured by a dashed line.
DRS: drag reduction system.

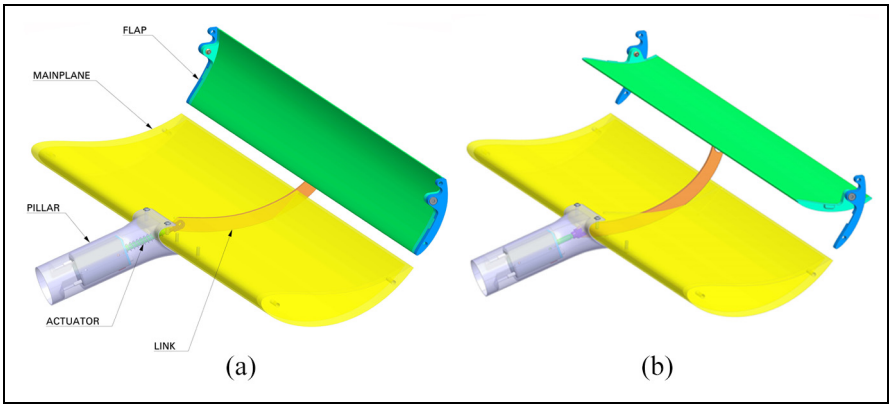

Figure 2. CAD model of the proposed DRS in (a) closed configuration and (b) open configuration.
DRS: drag reduction system.

surface and requires a great effort to the actuator because of the disadvantageous mechanism lever ratios. This solution was a first good approach for those cars employing a structural pillar to support the mainplane, for which the extra aerodynamic disturbance introduced by DRS was minimum. Another advantage of the push-up solution is the ease of access to hydraulic lines for maintenance.

Many cars without a pillar adopted the pod-rocker system (Figure 1(b)): the actuator and a part of the mechanism is included inside a pod, mounted over the mainplane. 'The actuator pulled on a rocker that increased the leverage of the piston, the rocker then is connected to the leading edge of the flap by link'.[15] Thanks to the rocker, this system requires a lower effort to the actuator and it eliminates any aerodynamic disturbance under the mainplane, since the hydraulic lines pass through the endplate. A better aerodynamic efficiency is paid through a higher cost of the mechanism and the need to open the hydraulic lines before removing the rear wing. Maintenance is easy for mechanical parts but more difficult for hydraulics.

Pod-pull setup is the evolution of pod-rocker one (Figure 1(c)): here the mechanism is simplified, replacing the rocker with a single link. Actuator must be supplied with a larger pressure, but this is not a limitation, thanks to the high-pressure hydraulics in use in the vehicle gearbox.

Mercedes used for a few years a DRS with the actuator mounted on the gearbox and a cable system that transfers the movement to the flap, through the end plates. This concept is aerodynamically excellent, but it introduces more friction and time delays in both opening and closing phases.

Among existing solutions, the best is certainly the pod-pull DRS that is currently used in Formula 1 cars. However, it has the disadvantage to require more effort from the actuator than the pod-rocker design and to generate more aerodynamic disturbance on the upper side of mainplane and flap, compared to the Mercedes DRS cable system.

The system proposed in this research and shown in Figure 2 can be seen as an evolution of the pod-pull system. It is conceived to ensure simultaneously a potentially lower actuation force and a less negative impact on the wing aerodynamics, keeping at the same time the executive simplicity and cost-effectiveness of the existing systems. It is also worth noting that the hydraulic lines pass through the pillar (they are not shown in Figure 2), similarly to all current racing cars equipped with a DRS.

The actuator is embedded inside the pillar and the mainplane (Figure 2). It is bolted to two aluminium inserts laminated inside the pillar (Figure 3). It is also supplied with a spring that allows closing the flap in the case of a failure of the actuator. The orange link transfers actuator motion to the flap. It has two needle roller bearings at its extremities in order to reduce friction. The entire link is a single, 4 mm thick, carbon fibre plate. Mainplane, flap and pillar are designed to be made of carbon fibre.

Figure 3(c) clarifies some design choice, made to minimize the actuator size. The segment $\overline{2_S3_S}$ is aligned with $\overline{3_S4_S}$ in order to minimize force components acting on the actuator along the perpendicular direction to its translation axis: these undesired forces may increase the actuator wear, reducing its useful life. The segments $\overline{2_S3_S}$ and $\overline{3_S4_S}$ are orthogonal to $\overline{4_S5}$. This condition, being equal to the length l_4 and the actuator force, guarantees the highest flap driving moment or the minimum actuator effort necessary to open the flap. The other geometric dimensions are chosen in order to achieve the right flap opening angle and to locate the actuator inside the mainplane and the pillar, or, in other words, to keep the actuator as close as possible to the mainplane leading edge.

CFD model validation

In order to validate our CFD approach for the computation of rear-wing aerodynamic forces, a two-dimensional (2D) simulation is preliminary performed with ANSYS 19.1 Academic on the NACA 4415 airfoil

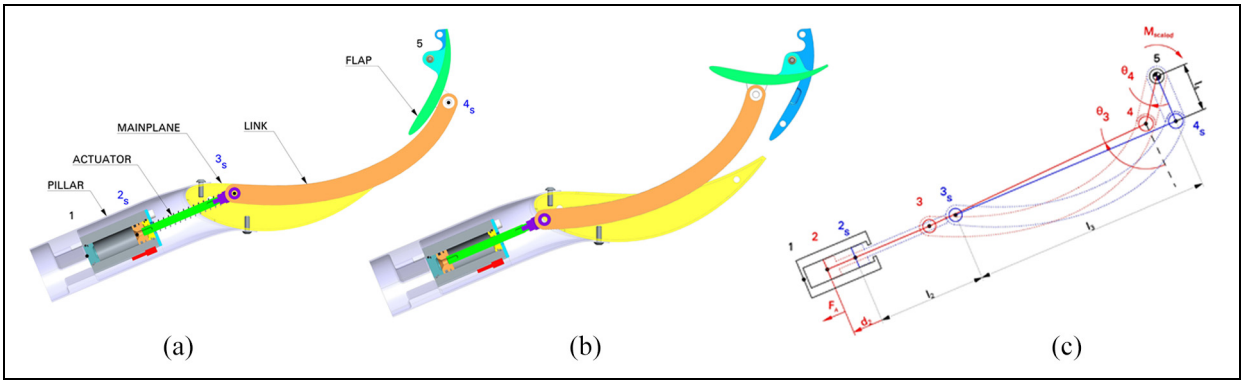

Figure 3. Cross section of the proposed DRS along the vehicle XZ plane in (a) closed configuration, (b) open configuration and (c) equivalent kinematic scheme.
DRS: drag reduction system.

(Figure 4(a)) that is chosen due to the availability of its theoretical and experimental data in terms of lift and drag coefficients. The theoretical aerodynamic characteristics of the airfoil are computed with XFOIL,[16] an interactive open-source programme for the design and analysis of subsonic isolated airfoils, while the experimental data are obtained from the results of a wind tunnel test campaign made by Ohio State University (OSU) on NACA 4415.[17] The comparison of CFD results with the airfoil available data leads to the choice of the turbulence model (TM), as the one that fits better the expected lift and drag coefficients. Two kinds of TMs, commonly used for automotive applications,[18] are investigated: the k–ω Standard (STD) and the k–ε STD. The starting point for the CFD analysis is the parametric 2D C-type structured mesh (Figure 4(b)), which takes the airfoil pitch angle as an input variable. For a given pitch angle, the model automatically predicts at first the airfoil incidence, than it regenerates the grid and finally performs the analysis in the new configuration, helping to speed up the iterative process. In the simulation, the airfoil pitch has been changed from $-10°$ to $+15°$, with positive values for nose-up attitude, and 0° for the horizontal chord position (represented in Figure 4(a)).

The mesh is made up of only quadrilateral elements. Variable aspect ratio and dimensions of the elements are arranged throughout the domain, in order to achieve a higher resolution for the regions in which the physical properties of the flow show higher variations, such as the boundary layer and the wake.

The chord length of 0.457 m and profile coordinates are the same of the wing tested by OSU. The simulation domain is 6.32 m long and 3.5 m high: these lengths are chosen after a first series of preliminary analyses, intended to reduce the domain only to the regions which show flow perturbations induced by the wing, with a static relative pressure close to zero at the boundaries. As for boundary conditions, the gauge outlet pressure is set to 0 Pa, no-slip condition is imposed on the wing, no-shear on the domain floor and ceiling. The

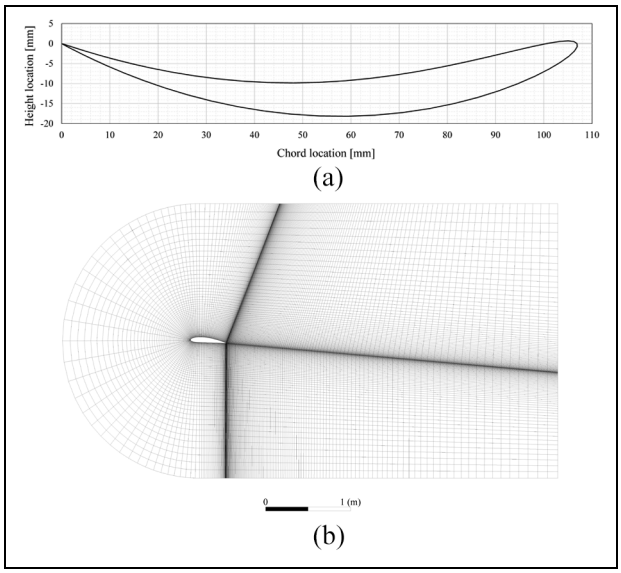

Figure 4. (a) NACA4415 airfoil at zero-pitch angle and (b) 2D C-type structured mesh of NACA4415 airfoil for a pitch angle of $+5°$.
2D:two-dimensional.

air inlet velocity is 50 m/s, corresponding to a Reynolds number of about 1.5×10^6, as that measured by OSU.

Figure 5 shows examples of simulation pressure output for airfoil pitch angle of $+5°$ and $+15°$ and for both the two TM analysed. Figure 6 sums up the comparison between lift and drag coefficients data coming, respectively, from XFOIL analytical data, OSU experimental tests and CFD analysis. It is apparent how both TMs and XFOIL perform well with pitch angles less than 5° in magnitude, with a simulation error less than 0.06 for the lift coefficient C_L and 0.005 for the drag coefficient C_D. With high positive pitch angles, the k–ω TM gives better results than the k–ε TM and XFOIL, with an error less than 0.18 for C_L and 0.005 for C_D. XFOIL performs better than CFD with high negative incidences, especially for the computation of drag coefficient. Nevertheless, this condition is not so relevant: it

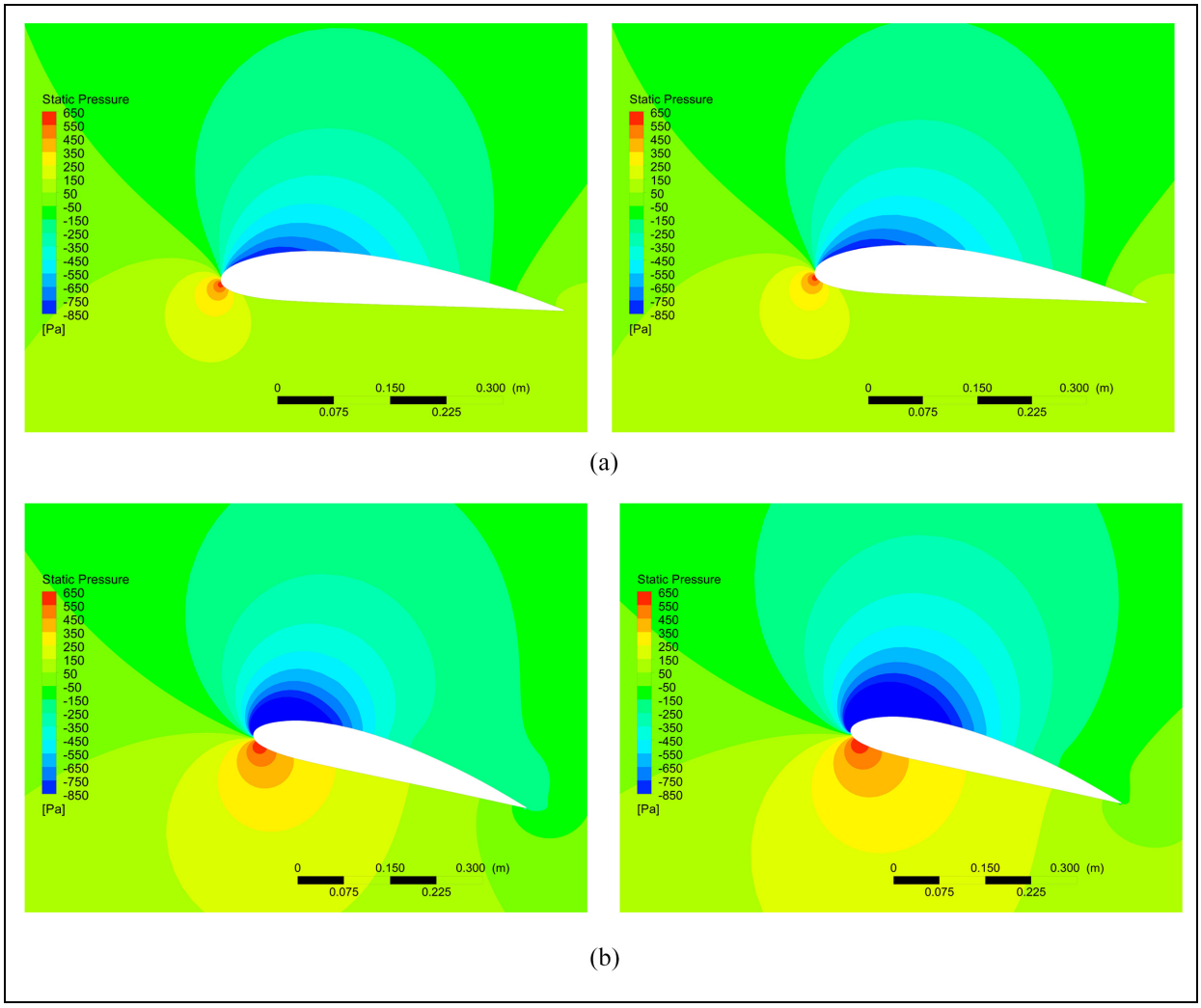

Figure 5. Static pressure contour plot of NACA4415 airfoil: k–ω TM on the left and k–ε TM on the right. (a) Pitch angle of +5° and (b) pitch angle of +15°.
TM: turbulence model.

has been investigated for completeness but it is generally a misuse for the airfoil. In common operating conditions, airfoil characteristics are better estimated by k–ω STD TM, so it will be used in the CFD analysis of the vehicle rear wing.

Rear-wing CFD model

The first input to the DRS design is the knowledge of the rear-wing structure and of the aerodynamic loads acting on it. Since the rear-wing design is not the aim of this work, a simplified rear wing is taken as a reference for the computations (Figure 7(a)). It is made up of two rectangular end plates (blue) with constant thickness of 7.5 mm; a mainplane (yellow) and flap (green) with a constant straight section along the entire span; a pillar (white) which covers the DRS hydraulic lines and a beam wing (red) that supports the entire wing.

Mainplane and beam wing have NACA 16520 profile. It has a higher thickness and camber than flap airfoil, which is a NACA 13509, thinner and less cambered in order to obtain enough drag reduction at low incidence. These two profiles and their relative position are selected as the most similar to typical racing profiles, after a comparison between various NACA airfoils and custom airfoils of different Formula vehicles (here not shown for confidentiality obligation). The simplified rear wing is expected to be low performing because NACA airfoils are less efficient than modified NACA designed by Formula car manufacturers; louvers and gurney flaps, typically employed on rear wings, are also ignored.

The rear-wing CFD model (Figure 7(b)) is simplified again for the simulation. Because of the bidimensionality of the analysis, the model is reduced to a general section of mainplane and flap along the vehicle longitudinal plane. The ground line of the simulation domain is coincident with the road, while the ceiling is 1.3 m over the wing. Inlet and outlet boundaries are, respectively, 1.2 m forwards and 3.5 m backwards the wing. As explained in the 'CFD model validation' section, domain dimensions are almost the minimum to

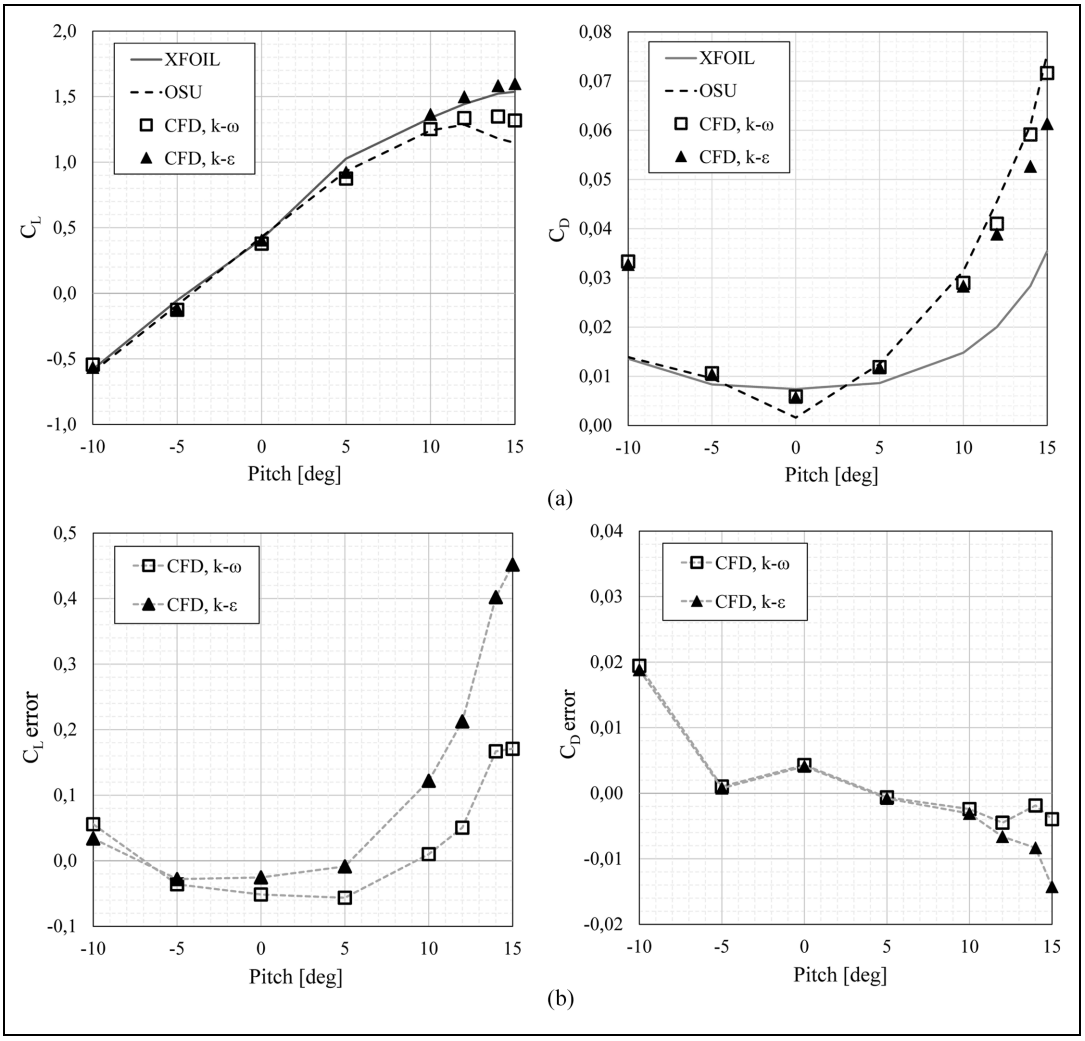

Figure 6. Comparison charts between the CFD study and OSU data: (a) lift and drag coefficients and (b) corresponding absolute errors.
CFD: computational fluid dynamics; OSU: Ohio State University.

guarantee a static relative pressure close to zero at the boundaries. Wing is assumed to have a 1 m span. Boundary conditions are kept as same as the CFD validation case, except for the ground that is declared as a no-slip wall, with a velocity of 50 m/s in the same direction of the airflow, to better simulate the road behaviour. Flap rotation angle was changed for each run from 0° to 70°, with a step of 10°. A flap angle of 0° corrresponds to the normally closed position (e.g. pitch angle equal to +70°), while 70° is the total rotation produced by DRS, which brings the flap in the fully opened configuration (e.g. pitch angle equal to 0°).

The simulation output are the aerodynamic longitudinal force F_X, the vertical force F_Z and the centre of pressure, individually computed for both flap and mainplane.

The angle at which the flap generates the minimum drag is 70° (Figure 8(a)). The negative sign in F_X is due to the coordinate system convention for which the x-axis points in the direction of vehicle longitudinal speed. Figure 8(b) shows that the fully opened position is close to be the flap zero-lift condition: in this configuration, a drag reduction of 85% is paid by a downforce decrease of 113% for the flap and of 39% for the entire wing (flap + mainplane) with respect to the fully closed position (Figure 9).

Figure 10(a) shows the influence of the rotation angle on the resultant aerodynamic force in terms of application point and direction. The resultant aerodynamic force is represented by an arrow coloured according to the rotation angle (see the inset of Figure 10(a)). As seen in this figure, at the angle of 70°, near to zero-lift angle, the resultant direction (black arrow) is near to be parallel, but not coincident, to the airfoil chord. In fact, cambered airfoils are characterized by a residual pitching moment at zero-lift angle, which results in a non-zero distance between resultant direction and profile chord, at the same angle.

Resultant force acting on the flap at various rotation angles can be translated to an equivalent aerodynamic moment around the flap rotation axis (Figure 10(b)). This moment will be useful in the DRS mechanism modelling, described in the 'Performance evaluation of the proposed system' section. Over 60° of flap rotation

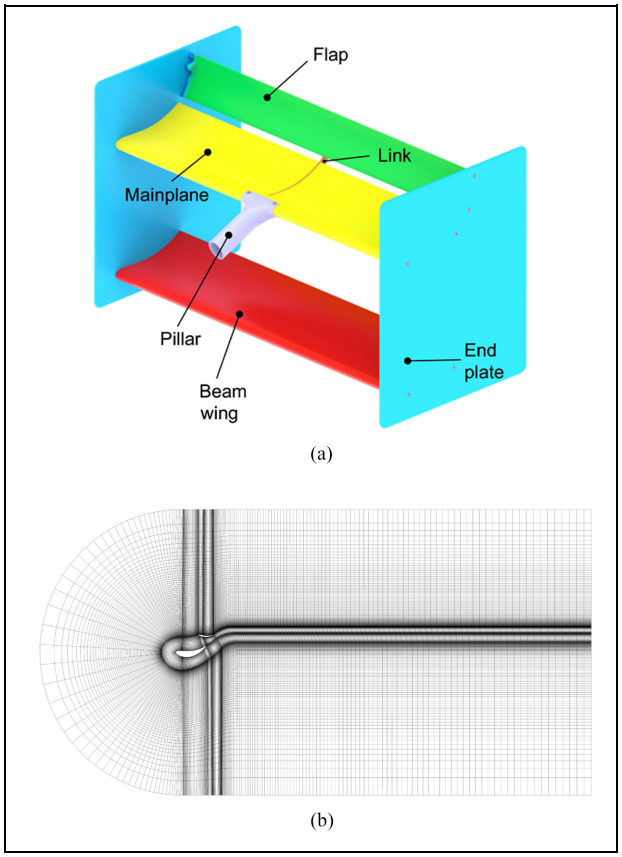

Figure 7. (a) CAD model of the reference rear wing and (b) 2D C-type structured mesh of the rear wing for a rotation angle of 70°.
2D: two-dimensional.

angle, the flap moment becomes negative and it tends to open the flap.

Performance evaluation of the proposed system

Previous sections have defined the aerodynamic stress field acting on the flap that defines the external load the DRS actuator needs to balance. In order to choose the actuator size and to prove its ability to open the flap, a quasi-static and a dynamic simulation are performed. The system has only one degree of freedom, which can be assumed as the actuator piston position d_2 (refer to Figure 3(c)). In the quasi-static simulation, for each piston position d_2, and so for each flap rotation angle θ_4, the aerodynamic moment M_{scaled} is applied to the flap, and the actuator force F_A that equilibrates the system is calculated (Figure 11(a)). The aerodynamic flap moment M_{scaled} can be computed by scaling the CFD resultant flap moment M_{CFD} (Figure 11(b)), obtained at 180 km/h (v_{CFD}), with the true vehicle speed of 208 km/h (v_{real}) when the vehicle enters in the DRS zone (see successive Figure 16(a)), assuming the term $C_X S$ constant

$$M_{scaled} = M_{CFD}\left(\frac{v_{real}}{v_{CFD}}\right)^2$$

The equilibrium equation can be easily computed with the application of the virtual works principle (refer to Figure 3(c))

$$F_A = -\frac{\partial\theta_4}{\partial d_2}\cdot M_{scaled}$$

The variables θ_3, θ_4 and d_2 are related through the following equations

$$\cos(\theta_3) = \frac{l_4}{l_3}(1-\cos(\theta_4))$$
$$d_2 = l_4\sin(\theta_4) + l_3(\sin(\theta_3)-1)$$

The maximum force claimed by the actuator is 335 N.

Finally, a dynamic simulation is performed to verify that the actuator can open the flap, calculating also the time necessary to open it. The DRS model considers mass (m_x) and inertias (I_x) of each component x, to compute inertial effects, along with the aerodynamic moment and a constant actuator force. Three different

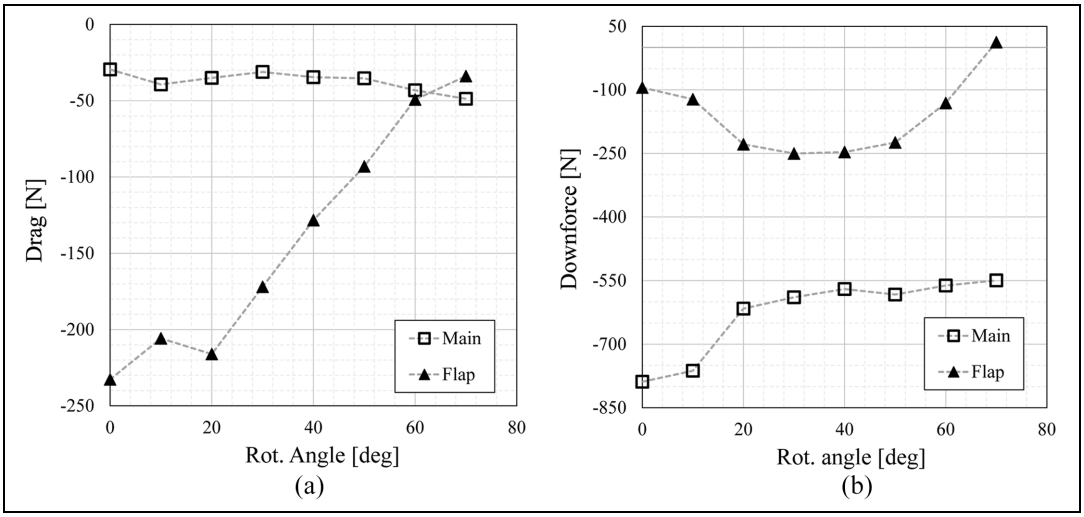

Figure 8. (a) Drag and (b) downforce for flap and mainplane at various flap rotation angles for an airflow speed of 50 m/s.

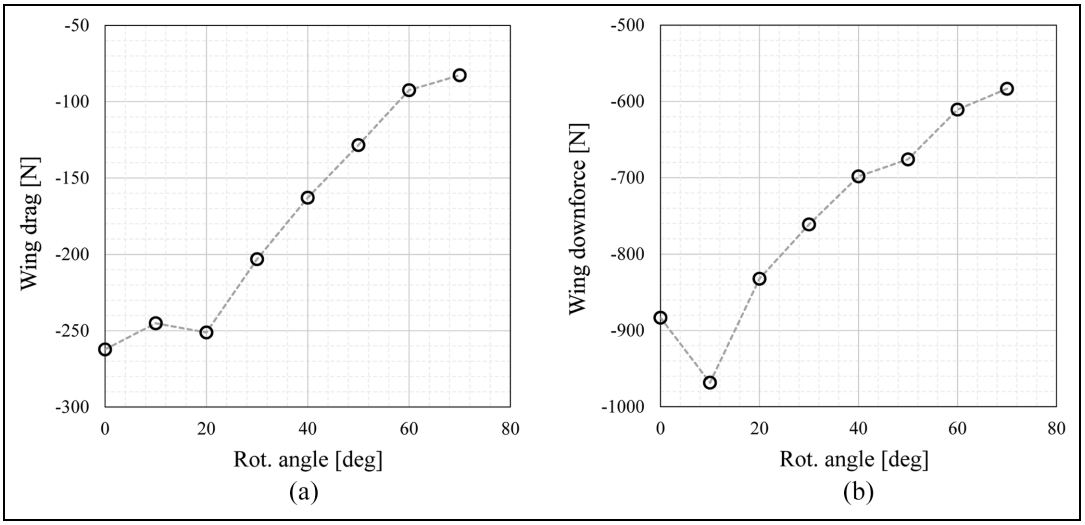

Figure 9. (a) Wing drag and (b) downforce at various flap rotation angles.

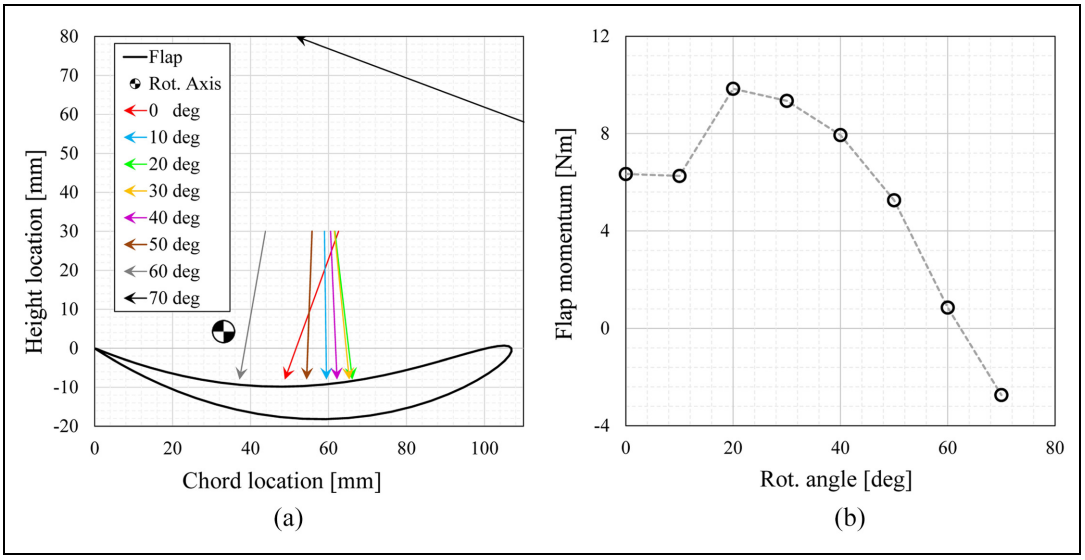

Figure 10. Wing net aerodynamic force as a function of the flap rotation angle: (a) aerodynamic resultant direction as measured by an observer attached to the flap: flap chord is horizontal and pass through zero-height line and (b) resultant flap moment reduced at the rotation axis.

runs with a constant actuator pull force produced, respectively, by pressures of 10, 20 and 30 bar have been performed. The dynamic equilibrium equation can be approximated by:

$$F_A + \frac{\partial \theta_4}{\partial d_2} \cdot M_{scaled} = M_{tot}(d_2)\ddot{d}_2 + \dot{M}_{tot}(d_2)\dot{d}_2^2$$

M_{tot} being the total mass inertia of the whole mechanism reduced to the actuator rod. The result of the integration of the forward dynamic problem is shown in Figure 12 expressed in terms of flap rotation angle as a function of time. The flap angular velocity (the curve slope) is lower at the beginning of the simulation, due to the inertia of the system, while the time to reach the opened position decreases for higher actuation pressures.

Overtaking manoeuvre

Consider a race car travelling on a levelled road as shown in Figure 13. The external forces acting on the vehicle include aerodynamic forces, inertial forces, gravitational forces and tyre forces. The longitudinal vehicle dynamic model assumes one degree of freedom corresponding to the position of the vehicle centre of mass and it allows one to simulate an overtaking manoeuvre.[19]

The aerodynamic forces are the longitudinal drag force F_{drag} and the vertical downforce, split into front and rear downforce, F_{downF} and F_{downR}. Other vertical forces are the vehicle total weight W and the normal reactions F_{zF} and F_{zR}, respectively, for the front and rear tyre contact patches. The remaining longitudinal

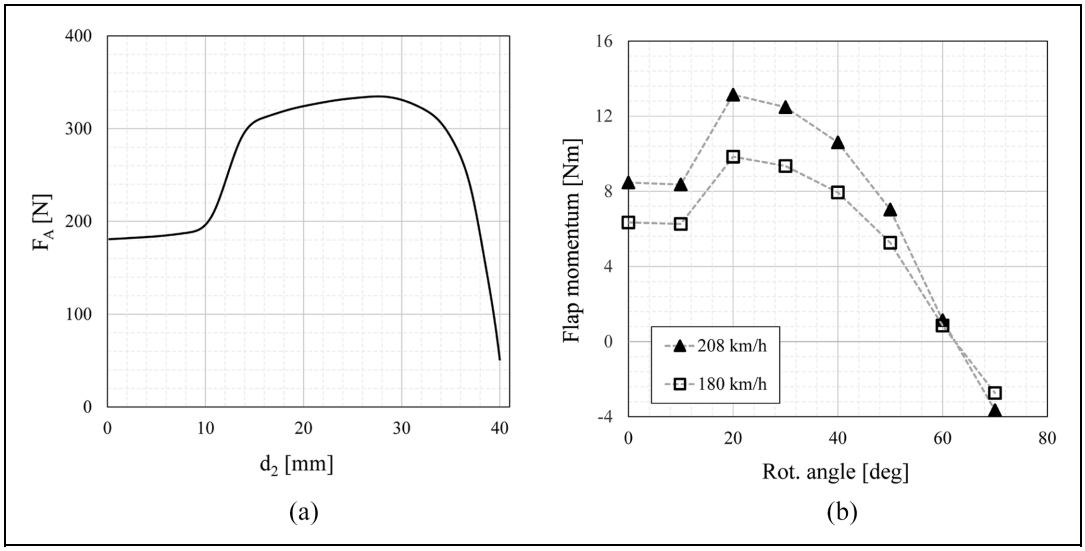

Figure 11. (a) Driving force F_A as a function of the piston position d_2 and (b) CFD and scaled resultant flap moment, respectively, at 180 and 208 km/h.
CFD: computational fluid dynamics.

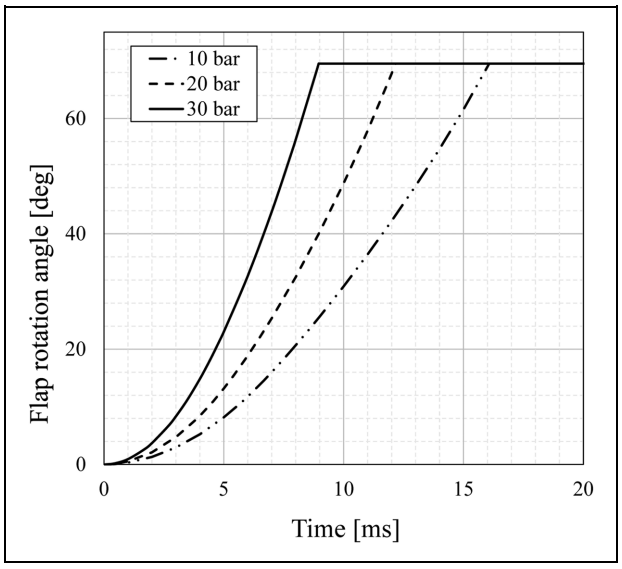

Figure 12. Simulation of flap opening with different actuator pressures.

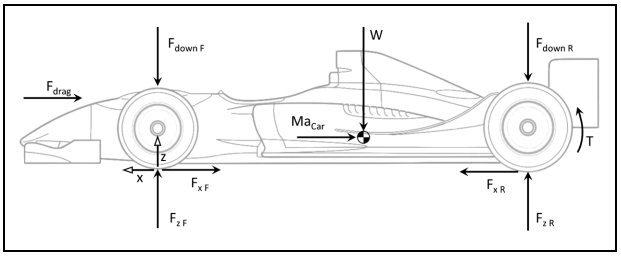

Figure 13. Longitudinal vehicle model.

forces are the inertial force Ma_{Car} and the tangential forces exchanged between tyres and road F_{xF} and F_{xR}. T is the torque developed by the rear axle. The longitudinal equilibrium gives as a result the following equation

$$F_{xR} - F_{xF} - F_{drag} = Ma_{Car} \tag{1}$$

By computing the equilibrium of moment for the rear tyre around wheel centre, it can be obtained

$$F_{xR} = \frac{T}{R} - \frac{I_{eq}}{R^2} a_{Car} \tag{2}$$

where R is the tyre radius and I_{eq} the equivalent moment of inertia that includes not only the actual moment of inertia of the wheels, I_w, but as well as those of the rotating masses of the gears and the shafts of the transmission, I_t, and of the engine I_e. The equivalent moment of inertia is then expressed as $I_{eq} = I_w + (I_t/\tau_1^2) + (I_e/\tau_1^2\tau_2^2)$; τ_1 and τ_2 being the transmission ratios along the driveline from the wheels to the engine.

Since race cars are usually rear wheel drive, F_{xF} accounts only for the rolling resistance. Here, its effect on the car acceleration is neglected. However, it will be included later in the calculation of the axle efficiency, required for the computation of the axle power.

Drag force can be replaced by

$$F_{drag} = \frac{1}{2}\rho_{air} C_X S v_{Car}^2 \tag{3}$$

where v_{Car} is the vehicle longitudinal speed, ρ_{air} is the air density, C_X the drag coefficient of the car and S the aerodynamic reference car surface.

After substitutions, the vehicle motion equation becomes

$$\frac{P_{axle}}{v_{Car}} - \frac{1}{2}\rho_{air} C_X S v_{Car}^2 = M_{eq} a_{Car} \tag{4}$$

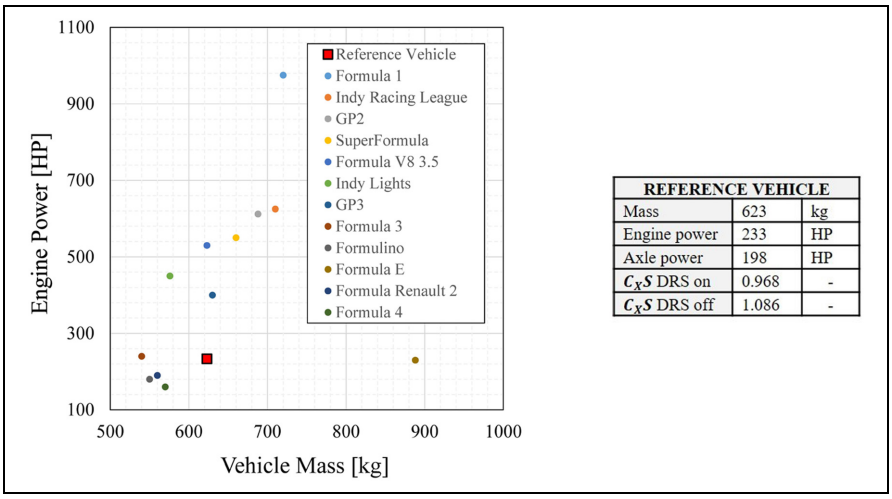

REFERENCE VEHICLE		
Mass	623	kg
Engine power	233	HP
Axle power	198	HP
C_XS DRS on	0.968	-
C_XS DRS off	1.086	-

Figure 14. Reference vehicle characteristics and its position among the main formula categories.

or equivalently

$$\frac{dv_{Car}}{dt} = \left(\frac{P_{axle}}{M_{eq}}\right)\frac{1}{v_{Car}} - \left(\frac{\rho_{air}C_XS}{2M_{eq}}\right)v_{Car}^2 \quad (5)$$

where the apparent mass of the car is introduced as $M_{eq} = M + (I_{eq}/R^2)$. The DRS is supposed to be installed on a reference vehicle with an apparent mass M_{eq}, engine power P_{axle} and C_XS averaged among those of the low-powered Formula vehicles (Figure 14), because of the low-performing NACA-based rear wing. Axle efficiency, a combined gearbox and tyre efficiency, is set as 0.85. The axle power P_{axle}, effectively available for traction, can be computed as the engine power times the axle efficiency. It is assumed that the axle power is constant during the entire passing manoeuvre.

The longitudinal drag force acting on the vehicle is the sum of the drag coming from both the rear wing and the rest of the car. The rear-wing drag is obtained from the CFD analysis described in section 'Rear-wing CFD model', whereas the drag produced by the rest of the car is calculated as an average among CFD data coming from some of the low-powered Formula vehicles (here not shown for confidentiality obligation). In addition, CFD data of other Formula vehicles have been computed at 50 m/s of longitudinal speed with simulation setup similar to that used in our rear-wing CFD. Known the total drag force on the vehicle, F_D, the car speed v (50 m/s) and air density ρ (assumed as 1.225 kg/m^3), C_XS (vehicle drag coefficient times reference surface) can be calculated as

$$C_XS = \frac{F_D}{\frac{1}{2}\rho v^2} \quad (6)$$

The composite drag coefficient has been computed for DRS in both opened and closed configurations. Equation (6) will be useful to calculate the vehicle drag force at different speeds in the overtaking simulation routine.

The reference track is Spa-Francorchamps in Belgium (Figure 15), since statistically it is the circuit

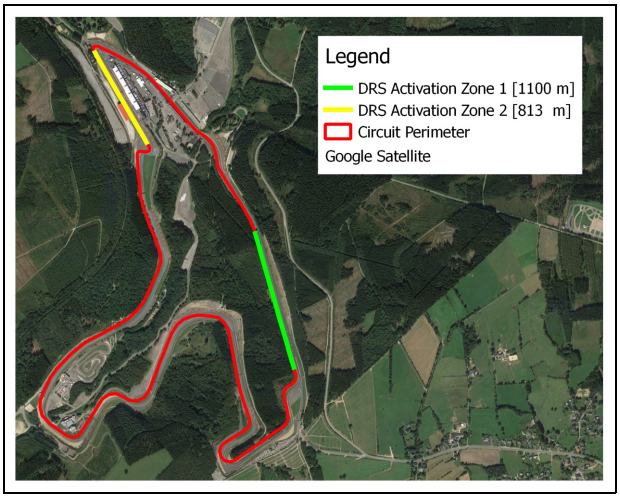

Figure 15. Google Satellite photo of Spa-Francorchamps track; DRS zone lengths have been measured in the WGS-84.
DRS: drag reduction system; WGS-84: World Geodetic System 1984.

in which a racing car could reach the higher speed in a DRS zone among all world circuits. In particular, speed records are reached in DRS zone 1. The selection of the world fastest DRS zone allows us to test the DRS mechanism in the worst conditions, as the aerodynamic forces acting on the flap are almost proportional to the square of vehicle speed. For the chosen track, the DRS zone 1 length is 1100 m, while the average speed v_0 for the reference vehicle, when it enters the same zone, is 208 km/h. The motion equation (5) has been numerically solved, imposing the initial velocity $v(0) = v_0$. The overtaking vehicle reaches the end of the DRS zone 1 of Spa in 5.13 s, outperforming the overtaken car in terms of speed and travelled distance, respectively, of 4.8 km/h (Figure 16(a)) and 14.1 m (Figure 16(b)). In conclusion, the proposed DRS allows an overtaking manoeuvre to be completed without making it too easy for the driver. In fact, typical final advantages admitted are in the range from 8 to 15 m.

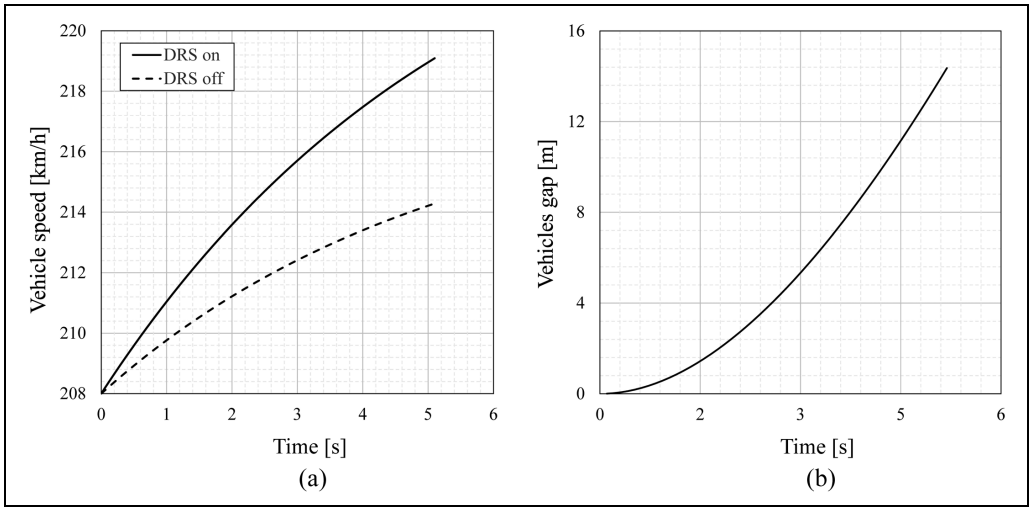

Figure 16. (a) Speed of two reference vehicles during overtaking manoeuvre at the DRS zone 1: solid black line refers to the vehicle with opened DRS, whereas the dashed black line refers to the same vehicle with closed DRS and (b) vehicle gap during the passing manoeuvre.
DRS: drag reduction system.

Conclusions and future works

In this paper, a full-design approach to active drag reduction was presented. It comprises four steps: (1) CFD simulation of the rear wing and computation of the corresponding aerodynamic forces, (2) validation and calibration of the wing fluid-dynamic model with existing wind tunnel experimental data, (3) design and optimization of the drive mechanism response to fulfil the required flap opening angle and actuation times and (4) simulation of the overtaking manoeuvre along a straight line using two identical cars having, respectively, DRS engaged and DRS disengaged.

Moreover, a new mechanism solution was introduced and described in detail. It generates a lower aerodynamic disturbance, keeping weight and cost comparable to current DRSs. As a matter of fact, it features a number of bearings and links that are equal or lower than that of existing solutions. In addition, it requires a moderate actuation effort, thus helping in limiting the actuator size, weight and cost. These features make the proposed system a promising candidate for future DRS implementations to be employed in a variety of formula categories.

An improvement to the described design process could be the extension of the CFD analysis to a three-dimensional model of the race car, in order to obtain more accurate results in terms of vehicle aerodynamic coefficients. More investigation may be devoted to the variation of engine power and gear shifting during the overtaking manoeuvre, enabling the validation of overtaking simulation results with test drive data.

Acknowledgements

The authors are in debt with Alessandro Fava (Dallara) for his precious insights on CFD analysis and DRS state of the art. G. Reina would like to dedicate this work to his "swift as the wind" son Lorenzo.

Declaration of conflicting interests

The author(s) declared no potential conflicts of interest with respect to the research, authorship and/or publication of this article.

Funding

The author(s) disclosed receipt of the following financial support for the research, authorship and/or publication of this article: The financial support of the project Autonomous DEcision making in very long traverses (ADE), H2020 (Grant No. 821988), is gratefully acknowledged.

ORCID iD

Giulio Reina https://orcid.org/0000-0003-1793-4419

References

1. Katz J. Aerodynamics of race cars. *Annu Rev Fluid Mech* 2006; 36: 27–63.
2. Tremayne D. *The science of formula 1 design*. London: Haynes Publishing, 2010.
3. Toet W. Aerodynamics and aerodynamic research in formula 1. *Aeronautic J* 2013; 117: 1–25.
4. Overtaking, applying science and commonsense, http://www.formula1-dictionary.net/overtaking.html
5. De Groote S. Aerodynamic study of the CDG concept, https://www.f1technical.net/articles/4577
6. Halley M. Kinetic energy recovery systems in formula 1. *ATZ Autotech* 2008; 8: 58–61.
7. Adjustable rear wing – Drag Reduction System (DRS), http://www.formula1-dictionary.net/drs_wing_rear_movable.html
8. Savkoor AR and Hapel H. Aerodynamic vehicle ride control with active spoilers. In: *Proceedings of the international symposium on advanced vehicle control (AVEC'96)*, Aachen, 1996, https://www.tib.eu/en/search/

id/BLCP%3ACN025954193/Aerodynamic-Vehicle-Ride-Control-with-Active-Spoilers/
9. Savkoor AR and Chou CT. Application of aerodynamic actuators to improve vehicle handling. *J Veh Syst Dyn* 1999; 32: 345–374.
10. Diba F, Barari A and Esmailzadeh E. Handling and safety enhancement of race cars using active aerodynamic systems. *Vehicle Syst Dyn* 2014; 52: 1171–1190.
11. Savkoor A, Manders S and Riva P. Design of actively controlled aerodynamic device for reducing pitch and heave of truck cabins. *Soc Automot Eng Japan Rev* 2001; 22: 421–434.
12. Schinestzki W, Schreiner D and Falcão C. Design of an automatic drag reduction system focusing on cooling for formula SAE vehicle. SAE Technical Paper 2016-36-0511, 2016.
13. Reina G and Foglia M. Modelling and handling dynamics of a wind-driven vehicle. *Vehicle Syst Dyn* 2019; 57: 697–720.
14. Reina G, Paiano M and Blanco-Claraco JL. Vehicle parameter estimation using a model-based estimator. *Mech Syst Signal Process* 2017; 87: 227–241.
15. Scarborough C. Analysis: DRS activation, http://forum.motorionline.com/topic/25080-drs-activation/
16. XFOIL. Subsonic airfoil development system, http://web.mit.edu/drela/Public/web/xfoil/
17. Hoffmann MJ, Reuss Ramsay R and Gregorek GM. Effects of grit roughness and pitch oscillations on the NACA 4415 airfoil. Technical Report, The Ohio State University, Columbus, OH, July 1996.
18. Taştan U. *Investigation of turbulence models used in automotive industry*. Master's Thesis, Middle East Technical University, Ankara, 2011.
19. Genta G and Genta A. *Road vehicle dynamics: fundamentals of modeling and simulation*. London: World Scientific Publishing, 2017.